JOURNAL OF GEOPHYSICAL RESEARCH, VOL. 115, D10205, doi:10.1029/2009JD012443, 2010

Parameterization of contrails in the UK Met Office Climate Model

A. Rap,[1] P. M. Forster,[1] A. Jones,[2] O. Boucher,[2] J. M. Haywood,[2] N. Bellouin,[2] and R. R. De Leon[3]

Received 7 May 2009; revised 7 December 2009; accepted 24 December 2009; published 19 May 2010.

[1] Persistent contrails are believed to currently have a relatively small but significant positive radiative forcing on climate. With air travel predicted to continue its rapid growth over the coming years, the contrail warming effect on climate is expected to increase. Nevertheless, there remains a high level of uncertainty in the current estimates of contrail radiative forcing. Contrail formation depends mostly on the aircraft flying in cold and moist enough air masses. Most studies to date have relied on simple parameterizations using averaged meteorological conditions. In this paper we take into account the short-term variability in background cloudiness by developing an on-line contrail parameterization for the UK Met Office climate model. With this parameterization, we estimate that for the air traffic of year 2002 the global mean annual linear contrail coverage was approximately 0.11%. Assuming a global mean contrail optical depth of 0.2 or smaller and assuming hexagonal ice crystals, the corresponding contrail radiative forcing was calculated to be less than 10 mW m^{-2} in all-sky conditions. We find that the natural cloud masking effect on contrails may be significantly higher than previously believed. This new result is explained by the fact that contrails seem to preferentially form in cloudy conditions, which ameliorates their overall climate impact by approximately 40%.

Citation: Rap, A., P. M. Forster, A. Jones, O. Boucher, J. M. Haywood, N. Bellouin, and R. R. De Leon (2010), Parameterization of contrails in the UK Met Office Climate Model, *J. Geophys. Res.*, *115*, D10205, doi:10.1029/2009JD012443.

1. Introduction

[2] Condensation trails, or simply contrails, are visible line-shaped high clouds that form behind an aircraft. As with all clouds, their presence causes an alteration in the Earth's radiation budget, via their shortwave (SW) albedo effect, i.e., they reduce the amount of SW radiation reaching the Earth, and their longwave (LW) greenhouse effect; that is, they reduce the amount of LW radiation leaving Earth to space. The balance between these two competing effects is strongly dependent on the cloud optical properties and altitude (temperature) [*Fu et al.*, 2000]. While for all cloud cover in general, the cooling effect dominates the warming effect, the opposite has been shown to be the case for thin cirrus and contrails.

[3] The theory behind the contrail formation process is well understood since the publication of the first two papers that provided the explanation of this process based on thermodynamic theory, namely those by *Schmidt* [1941] and *Appleman* [1953]. Nowadays it is therefore known that contrails form under liquid water saturation conditions as a result of heat and water vapor mixing between the warm and moist exhaust and the cool ambient air. When they form in dry unsaturated air, contrails are usually short-lived, but when the ambient relative humidity exceeds ice saturation, they persist and can develop into extended cirrus cloud layers [see, e.g., *Schumann*, 1996]. Existing studies have shown that for these persistent contrails, their daily average LW radiative forcing (RF) effect is larger than their SW effect, meaning that contrails cause a positive net RF, and therefore a warming [see, e.g., *Meerkötter et al.*, 1999]. The magnitude of this net positive RF estimated by various studies for the air traffic of the year 1985, varies from a value of 2.0 mW m^{-2} [*Stuber and Forster*, 2007] to a value of 17 mW m^{-2} [*Minnis et al.*, 1999]. According to the Intergovernmental Panel on Climate Change (IPCC) fourth assessment [*Forster et al.*, 2007], the linear contrail radiative forcing for the year 2005 is estimated at 10 mW m^{-2}, with an uncertainty factor of 3 caused by a low level of current scientific understanding. This represents an important contribution, i.e., approximately 20%, of the total aviation RF. The high uncertainty factor still present in our estimates of contrail RF is mainly due to the limited knowledge of contrail optical properties and contrail coverages. When estimating global contrail RF, most available models assume constant optical properties for contrails. Currently there are only two climate model approaches that

[1]Institute for Climate and Atmospheric Science, School of Earth and Environment, University of Leeds, Leeds, UK.
[2]Met Office Hadley Centre, Exeter, UK.
[3]Centre for Air Transport and the Environment, Manchester Metropolitan University, Manchester, UK.

0148-0227/10/2009JD012443

have the ability of considering a geographical and temporal variability for contrail optical depths, namely the *Ponater et al.* [2002] model, with amendments by *Marquart and Mayer* [2002], and the *Burkhardt and Kärcher* [2009] contrail cirrus model, both hosted by the ECHAM4 climate model. As air traffic is expected to experience a significant increase in the future, the contrail warming effect may become stronger and therefore the development of more reliable models that can accurately estimate contrail formation and their radiative impact is considered important. Also, more than one GCM configuration is desirable to provide reliable error estimates, due to the different performance of cirrus parameterizations in GCMs, as indicated by, for example, *Lohmann and Kärcher* [2002] and *Waliser et al.* [2009].

[4] The aim of the current study is to develop a new linear contrail parameterization by adapting the contrail parameterization from *Ponater et al.* [2002] to the second version of the UK Hadley Centre Global Environmental Model (HadGEM2) [*Collins et al.*, 2008]. This provides the research community with an additional GCM tool for estimating the impact of contrails on the Earth's radiative budget and climate, and an alternative development platform for advanced research on the global impact of aircraft induced cloudiness. This paper addresses only the radiative forcing aspects of the parameterization. In a planned follow-up paper the full climate impact of these parameterized contrails will be evaluated.

[5] Section 2 of the present paper describes the methodology of our contrail parameterization. The results obtained for the contrail coverage, optical depth, and radiative forcing are then presented in sections 3, 4, and 5, respectively. Finally, section 6 discusses some of the main results and summarizes the conclusions of this study.

2. Contrail Parameterization Within HadGEM2

[6] This section describes the implementation of the contrail parameterization within the Hadley Centre climate model HadGEM2. Section 2.1 briefly presents the host climate model, section 2.2 describes the details of our parameterization and section 2.3 shows some benchmark calculations for the evaluation of the radiation code employed in this study.

2.1. Host Climate Model: HadGEM2

[7] The host climate model for our contrail parameterization is the Hadley Centre climate model HadGEM2 [*Collins et al.*, 2008]. The model generates its own meteorology based on greenhouse gases, aerosol emissions and land use distribution for the year 2000. The sea surface temperatures and sea ice are from the AMIP II observed climatology [*Hurrell et al.*, 2008], averaged over the 1978–1995 period.

[8] The radiation scheme of HadGEM2 is that of *Edwards and Slingo* [1996], which will be described in section 2.3. The cloud scheme within HadGEM2 is the same with the one from HadGEM1 [see *Martin et al.*, 2006]. This is based on the *Smith* [1990] scheme, in which cloud water and cloud amount are diagnosed from total moisture and liquid water potential temperature using a triangular probability distribution function. Also, the main assumption regarding the interaction with radiation and clouds in the model is that clouds consist of four components (stratiform water and ice, convective water and ice) and they are treated as plane parallel (no 3D effects) with a maximum random overlap assumption.

[9] The HadGEM2 experiments employ a resolution configuration of 192 (longitude) × 145 (latitude) × 38 (altitude). This differs from the resolution of the off-line radiation code calculations employed in sections 2.3 and 5.1.

2.2. Contrail Parameterization

[10] For the contrail parameterization within HadGEM2 we adopt a similar methodology to the one developed by *Ponater et al.* [2002] for the ECHAM4 climate model. Based on contrail formation thermodynamics, the maximum temperature and minimum relative humidity thresholds necessary for contrails to form depend only on the ambient temperature, pressure and relative humidity, as well as on the emission index of water vapor, the specific heat of fuel combustion and on the propulsion efficiency of the aircraft engine.

[11] The threshold temperature (in K) for contrail formation used in our parameterization is the one estimated by *Schumann* [1996], namely

$$T_{\mathrm{contr}} = 226.69 + 9.43\ln(G - 0.053) + 0.72\ln^2(G - 0.053), \tag{1}$$

where G is the slope of the mean phase trajectory in the turbulent exhaust field on an absolute temperature versus water vapor partial pressure diagram. G has the unit of Pa K^{-1} and is given by

$$G = \frac{EI_{H_2O} c_p p}{\epsilon Q(1-\eta)}, \tag{2}$$

where $EI_{H_2O} = 1.25$ is the emission index of water vapor, $c_p = 1004$ J $kg^{-1}K^{-1}$ is the isobaric heat capacity of air, p is the ambient air pressure, $\epsilon = 0.622$ is the ratio of molecular masses of water and dry air, $Q = 43$ MJ kg^{-1} is the specific combustion heat, and $\eta = 0.3$ is the average propulsion efficiency of the jet engine.

[12] The critical relative humidity, r_{contr}, for contrail formation at a given ambient temperature T can then be calculated as

$$r_{\mathrm{contr}}(T) = \frac{G(T - T_{\mathrm{contr}}) + e_{\mathrm{sat}}^{\mathrm{liq}}(T_{\mathrm{contr}})}{e_{\mathrm{sat}}^{\mathrm{liq}}(T)}, \tag{3}$$

where $e_{\mathrm{sat}}^{\mathrm{liq}}(T)$ is the saturation pressure of water vapor with respect to the liquid phase, at a given temperature T.

[13] As in the *Ponater et al.* [2002] study, in order to adapt the theory of local contrail formation to the HadGEM2 cloud scheme, we define a modified relative humidity threshold r^*_{crit}, by combining the theoretical threshold r_{contr} with the threshold $r_{\mathrm{crit}} = 0.8$ controlling the initiation of cirrus formation in HadGEM2,

$$r^*_{\mathrm{crit}} = r_{\mathrm{contr}} \cdot r_{\mathrm{crit}}. \tag{4}$$

[14] Following *Smith* [1990], the UK Met Office Climate Model parameterization of natural cirrus coverage is based

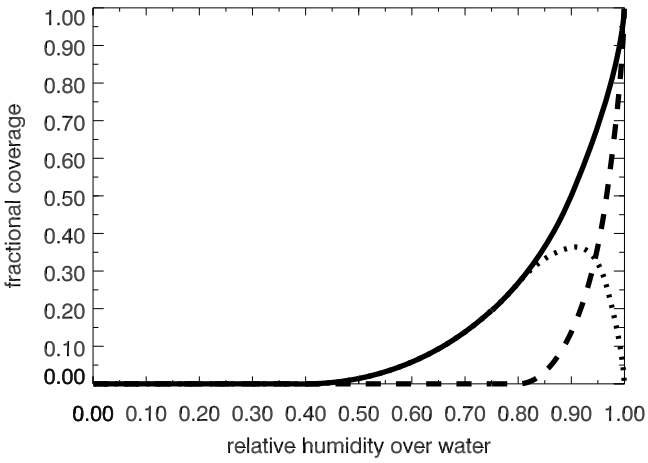

Figure 1. Parameterization of the fractional coverage of natural cirrus clouds b_{cirrus} (dashed line), potential contrails $b_{\text{contr}}^{\text{potential}}$ (dotted line), and the sum of total natural cirrus and contrails $b_{\text{total}}^{\text{potential}}$ (solid line) in case of $r_{\text{contr}} = 0.5$, $r_{\text{crit}} = 0.8$ and constant q_{cf}.

on the assumption of a symmetric triangular probability distribution function (PDF) of the total water saturation excess, s, around its grid box mean. Details are given by *Wilson and Gregory* [2003] and *Wilson* [2007]. Using the *Smith* [1990] cloud fraction formula, the natural cirrus cloud coverage (b_{cirrus}) is then given by

$$b_{\text{cirrus}} = \begin{cases} 0 & , \text{if} \quad Q_N \le -1 \\ \frac{1}{2}(1+Q_N)^2 & , \text{if} \quad -1 < Q_N \le 0 \\ 1-\frac{1}{2}(1-Q_N)^2 & , \text{if} \quad 0 < Q_N < 1 \\ 1 & , \text{if} \quad 1 \le Q_N \end{cases}, \tag{5}$$

where

$$Q_N = \frac{q_{cf}}{b_{si}} - \left(\frac{1-r_{\text{water}}}{1-r_{\text{crit}}}\right), \tag{6}$$

with q_{cf} being the ice water content and $b_{si} = (1 - r_{\text{crit}})\, q_{\text{satwater}}$ the half width of the triangular PDF in s. This width is defined such that the condensation in the grid box occurs when the grid box mean relative humidity over water $r_{\text{water}} = q/q_{\text{satwater}}$ equals the prescribed r_{crit}.

[15] It should be noted here that the *Smith* [1990] ice cloud scheme employs the saturation humidity with respect to water, and not with respected to ice. This was chosen primarily to produce consistency in cloud fractions when liquid water cloud was homogeneously frozen to ice [see *Wilson*, 2007], and in our case means that equation (4) is consistent, all three relative humidities being defined over water.

[16] Employing r_{crit}^{*} from equation (4), but maintaining the same width b_{si} of the triangular PDF, we define

$$Q_N^{*} = \frac{q_{cf}}{b_{si}} - \left(\frac{1-r_{\text{water}}}{1-r_{\text{crit}}^{*}}\right). \tag{7}$$

As pointed out by *Burkhardt et al.* [2008], when developing a new coverage parameterization (in our case, linear contrail coverage), it is important to maintain consistency with the existing natural cloud coverage parameterization, by employing in both cases the same PDF of total water, with the same fixed width.

[17] With this new Q_N^{*}, we obtain a potential cloud coverage for all high clouds ($b_{\text{total}}^{\text{potential}}$), including both natural cirrus and contrails, by replacing Q_N with Q_N^{*} in equation (5). We can then define a potential cloud coverage for contrails only as

$$b_{\text{contr}}^{\text{potential}} = b_{\text{total}}^{\text{potential}} - b_{\text{cirrus}}. \tag{8}$$

[18] Figure 1 shows b_{cirrus}, $b_{\text{contr}}^{\text{potential}}$ and $b_{\text{total}}^{\text{potential}}$ as functions of the grid box mean relative humidity with respect to water for the case when $r_{\text{contr}} = 0.5$ and $r_{\text{crit}} = 0.8$. It can be seen that the potential contrail cover reaches its maximum at values comparatively larger than those from *Ponater et al.* [2002] as shown in their Figure 1.

[19] The final parameterized contrail coverage is then calculated using the following expression:

$$b_{\text{contr}} = \gamma \cdot D \cdot b_{\text{contr}}^{\text{potential}}, \tag{9}$$

where γ is a nonphysical scaling factor obtained by calibrating the temporal and spatial average of contrail coverage to observed conditions, and D is the local distance flown that allows us to account for the dependency of the contrail coverage on the density of air traffic. The contrail coverage parameterized in this way (b_{contr}) is a three-dimensional field, defined for every (longitude × latitude × altitude) grid box in the model.

[20] For the distance flown data D, we use the AERO2K global air traffic inventory [*Eyers et al.*, 2004]. This inventory provides the total distance flown by aircraft on a three-dimensional grid for each month of the year 2002. Also, for one week in June, the data is provided for four 6-hourly time periods starting at midnight GMT. We apply this diurnal variation from that week in June to the distance flown for all months.

[21] It should also be mentioned that the parameterization considers only contrails that persist for at least 30 minutes, i.e., one model time step. An implicit contrail persistence criterion is incorporated into the scheme using the same approach as that of *Ponater et al.* [2002]; that is, if there is no contrail ice water formation at some time step, then the contrail coverage is reset to zero.

[22] The contrail optical depth, τ, is calculated as the integral over vertical levels of the contrail specific extinction coefficient, k_{ext} in m^2kg^{-1}, weighted by the contrail mass-mixing ratio, MMR in kg kg^{-1}, following:

$$\tau(\lambda) = \int_z k_{\text{ext}}(\lambda)\text{MMR}(z)\rho(z)dz, \tag{10}$$

where λ is the wavelength, z is the vertical coordinate (in m), and ρ is the air density (kg m^{-3}). Specific extinction coefficients are obtained using the contrail size distribution and optical properties of *Strauss et al.* [1997]. Throughout this paper, the optical depth is assumed to be independent of

Table 1. Global Mean Radiative Forcing at the Top of the Atmosphere for a 100% Homogeneous Contrail Coverage at 250 hPa Indicating the Dependence of Ice Crystal Shape[a]

Ice Crystal Shape	Reference	LW	SW	Net
Spheres	*Meerkötter et al.* [1999]	51.6	−13.4	38.2
	this study	44.2	−11.0	33.2
Aggregates	this study	46.4	−27.9	18.5
Hexagonal cylinders	*Meerkötter et al.* [1999]	51.5	−22.0	29.5
	Myhre and Stordal [2001]	45.6	−25.2	20.4
	Stuber and Forster [2007]	44.2	−20.3	23.9
	this study	43.7	−24.1	19.6

[a]Unit is W m^{-2}. Studies are for July values and for an optical depth of 0.52 at 0.55 μm and an ice water content of 21 mg/m^3.

wavelength and is given at 0.55 microns. Finally, it should be mentioned that the contrail mass-mixing ratio MMR is a dimensionless variable defined as the product of the ice mass mixing ratio and the contrail fraction.

2.3. Benchmark Calculations

[23] Once contrail coverage and optical depth distributions are generated, these can then be used in order to evaluate the contrail RF by employing a radiative transfer model. The model used in this study is the Edwards-Slingo radiation code [see *Edwards and Slingo*, 1996], in both its off-line and on-line (within HadGEM2) versions. The climate model based version of this code employs 6 bands in the shortwave and 9 bands in the longwave and adopts a delta-Eddington 2 stream scattering solver at all wavelengths. As noted by *Marquart and Mayer* [2002], not accounting for scattering by contrail in the longwave can be a source of error.

[24] In order to evaluate the performance of this radiation code for estimating the contrail RF we first perform some test calculations where the contrail cover is represented by a homogeneous constant global cloud cover of cirrus. As in work by *Meerkötter et al.* [1999], a 100% homogeneous contrail coverage is assumed at 250 hPa, with a constant optical depth $\tau = 0.52$ at 0.55 μm, an ice water content IWC = 21 mg m^{-3}, and a generalized mean effective size D_{ge} = 23μm. Following *Fu* [1996], the generalized mean effective size is given by

$$D_{ge} = \frac{2\sqrt{3}\mathrm{IWC}}{3\rho_i A_c}, \tag{11}$$

where $\rho_i = 0.9167$ g cm^{-3} is the ice density and A_c is the total cross-sectional area of the particle per unit volume. Also, the effective radius (r_e) is given by [see *Fu*, 1996]

$$r_e = \frac{3\mathrm{IWC}}{4\rho_i A_c} \tag{12}$$

and can therefore be related to D_{ge} in the form

$$r_e = \frac{3\sqrt{3}}{8} D_{ge}. \tag{13}$$

[25] Three different ice particle shapes are considered, namely spheres, aggregates, and hexagonal cylinders. Using the off-line Edwards-Slingo code with the 144 (longitude) × 72 (latitude) × 23 (altitude) resolution, the LW, SW and net RFs at the top of the atmosphere can be estimated. Table 1 shows the results obtained by the model for the global mean RFs, compared with similar cases presented by *Meerkötter et al.* [1999], *Myhre and Stordal* [2001], and *Stuber and Forster* [2007]. As already shown by these earlier studies, we note that the shape of the ice particles plays an important role, with aggregates and hexagonal cylinders exerting significantly less net RFs than spherical ice particles. This difference in the net RFs is mainly due to the different influences on the SW radiative flux, as the shape does not change the LW fluxes significantly. The choice of the ice particle shape is therefore an important factor in estimating the contrail RF. In the remainder of this paper we use hexagonal cylinders in all calculations. In terms of comparing our model results with those presented in the other three publications, it can be seen that the RFs obtained by our Edwards-Slingo code are broadly consistent with those reported by the other authors, although due to SW and LW forcing cancellation, net differences in forcing can be as large as 30%.

[26] Another test for the radiation code is performed by considering the *Myhre and Stordal* [2001] case, also repeated by *Stuber and Forster* [2007], where a 1% homogeneous contrail coverage is assumed at 250 hPa, with an optical depth $\tau = 0.3$ at 0.55 μm, an ice water content IWC = 21 mg m^{-3}, and a generalized effective size D_{ge} = 23μm. For these calculations, the natural clouds are based on monthly averaged distributions for the 1983–2002 period, for low-level, midlevel and high-level cloud from the International Satellite Cloud Climatology (ISCCP) project. For comparison, *Stuber and Forster* [2007] also used ISCCP data, whilst *Myhre and Stordal* [2001] employed 1996 natural clouds from the European Centre for Medium-Range Weather Forecasts (ECMWF) analysis.

[27] Table 2 shows the results obtained in this case, for both clear-sky and all-sky conditions, which are remarkably similar to those reported by the above two papers. Both the LW and SW contrail RFs are reduced by the presence of clouds, via the cloud masking effect. However, since this effect has similar magnitudes in the LW and SW, this results in the clouds having a very small effect on the net contrail RFs.

[28] For purely technical reasons, on-line contrail RF calculations within HadGEM2 are easier to perform if the contrail is artificially considered as a new aerosol species, rather than an ice cloud. The only shortcoming of such a technical assumption is that, for aerosols, the model does not have an "aerosol fraction". Therefore, if we are to include contrails as aerosols in HadGEM2 RF calculations, then we

Table 2. Radiative Forcing at the Top of the Atmosphere for a 1% Homogeneous Contrail Coverage at 250 hPa[a]

	Clear Sky			All Sky		
Reference	LW	SW	Net	LW	SW	Net
Myhre and Stordal [2001]	0.27	−0.15	0.12	0.21	−0.09	0.12
Stuber and Forster [2007]	0.25	−0.12	0.13	0.19	−0.06	0.13
this study	0.27	−0.15	0.12	0.22	−0.10	0.12

[a]Unit is W m^{-2}. Studies are for July values, an optical depth of 0.3 at 0.55 μm, an ice water content of 21 mg/m^3, and hexagonal cylinders ice particles.

Table 3. Radiative Forcing at the Top of the Atmosphere for 1%, 10%, and 100% Homogeneous Contrail Coverage at 250 hPa[a]

		Clear Sky			All Sky		
Optical Depth	Coverage	LW	SW	Net	LW	SW	Net
0.3	1%	0.27	−0.15	0.12	0.22	−0.11	0.11
0.003	100%	0.31	−0.19	0.12	0.25	−0.14	0.11
0.3	10%	2.74	−1.5	1.24	2.2	−1.04	1.14
0.03	100%	3.05	−1.8	1.25	2.44	−1.28	1.16
0.52	1%	0.44	−0.24	0.2	0.36	−0.17	0.19
0.0052	100%	0.53	−0.32	0.21	0.44	−0.24	0.2
0.52	10%	4.37	−2.37	2.0	3.5	−1.68	1.82
0.052	100%	5.24	−3.07	2.17	4.2	−2.17	2.03

[a]Unit is W m^{-2}. Studies are for July values, hexagonal cylinders ice particles and various optical depths.

must be able to control the contrail coverage (cloud fraction) by another parameter, that is present in the aerosol radiative transfer scheme of the model. The best candidate for such a parameter is the aerosol optical depth. Thus, we want to check if, from a radiative transfer point of view, it is reasonable to assume that instead of having a b_{contr} contrail coverage of optical depth τ, we can assume of having a 100% contrail coverage of optical depth $b_{\text{contr}}\tau$. Technically, this would allow the treatment of the contrails as aerosols. We consider four such coupled cases: the first one with 1% contrail coverage and $\tau = 0.3$, compared with 100% contrail coverage and $\tau = 0.003$, and the second one for a 10% contrail coverage with $\tau = 0.3$, compared with 100% contrail coverage and $\tau = 0.03$. The third and fourth cases consider similar coverages but optical depths of $\tau = 0.52$, $\tau = 0.052$ and $\tau = 0.0052$. Again, both clear-sky and all-sky conditions are investigated.

[29] The results presented in Table 3 show that when considering a 100% contrail coverage, with a correspondingly smaller optical depth, the magnitude for both the LW and SW forcings increases, compared with the case when 1% or 10% contrail coverages are assumed but with higher optical depths. These differences would affect the forcing diurnal variations and may affect the climate response. However, for the net forcings, these differences virtually cancel each other, meaning that controlling the contrail fraction in the model by correspondingly altering the optical depth is not an unreasonable assumption for daily averaged forcing estimates. It should also be mentioned that when doing this scaling on the optical depth the other contrail optical properties remain unchanged.

3. Contrail Coverage

[30] With the contrail parameterization described in section 2.2 incorporated in the HadGEM2 GCM, a 5 year simulation was performed. The averaged contrail cover over these 5 years represents a fractional coverage within each model grid box for all contrails. Integrating the contrail coverage vertically for all model levels, using the random overlap principle, a two-dimensional coverage distribution is obtained. However, this distribution needs to be calibrated using some available observations for contrail coverage, via the nonphysical scaling factor γ from equation (9).

[31] The observations employed for calibration in this study are those reported by *Bakan et al.* [1994], which were also used in other studies such as those by *Ponater et al.* [2002] and *Rädel and Shine* [2008]. These observations are 24 h means of visual inspection of quicklook photographic prints from NOAA satellites infrared images for the geographical area of 30°W to 30°E and 35°N to 75°N (referred to here as the "Bakan" area). The *Bakan et al.* [1994] study uses observations from two periods, namely 1979–1981 and 1989–1992, while the AERO2K traffic inventory we use in this paper corresponds to the year 2002. According to *Rädel and Shine* [2008], a factor of 2 is a good approximation of the air traffic increase in the "Bakan" area from 1985 (the year considered representative for the *Bakan et al.* [1994] observations) to 2002. This factor of 2 is therefore taken into account when scaling the contrail coverage produced by the parameterization to the observed average coverage for the "Bakan" area, which was 0.375% for the 1985 air traffic.

[32] For the calculation of the scaling factor γ from equation (9), we only consider the visible contrails, where the same criterion for visible contrails as in work by *Ponater et al.* [2002] is used; that is, the contrails must have an optical depth larger than 0.02 and they must not be disguised by natural clouds (the natural clouds coverage in the layers above or immediately below must not be larger than 80%).

[33] Once the scaling factor is chosen, other observed coverages reported by some existing studies for various geographical regions can be investigated (see Figure 2). One such a region is the western Europe area of 10°W to 23°E and 40°N to 56°N from *Meyer et al.* [2002], where data of the Advanced Very High Resolution Radiometer (AVHRR) sensor onboard the NOAA 14 satellite was analyzed for the 1995–1997 period using an operational contrail detection algorithm. The 1985 average contrail coverage for this region reported by *Meyer et al.* [2002] is 0.5%, while *Bakan et al.* [1994] and *Stuber and Forster* [2007] reported values of approximately 0.7% and 0.9%, respectively. Our value for the same region is 0.97% for the year 1985.

[34] For the eastern Pacific area of 120°W to 150°W and 25°N to 55°N the average contrail coverage during May, August and November 2002 and February 2003 reported by *Minnis et al.* [2005] was 0.31%. Their calculation was based on 1 km window channel data from the AVHRR on the NOAA 16 satellite, that was analyzed using a automated detection method from *Mannstein et al.* [1999]. Using the AERO2K air traffic data, combined with ECMWF analysis, *Rädel and Shine* [2008] found a 2002 mean contrail coverage for the same region of 0.27%, while the value found using our current study is 0.23%.

[35] *Meyer et al.* [2007] used remote sensing observations from the NOAA/AVHRR satellite corresponding to the year 1998, analyzed by a fully automated contrail detection algorithm to produce contrail coverage for two regions covering Japan (125.625°E to 148.125°E and 29.689°N to 48.245°N) and Thailand (91.88°E to 121.875°E and 0°N to 25°N); for these two regions their observed coverages were 0.25% and 0.13%, respectively, while our parameterization generates coverages corresponding to the year 2002 of 0.17% and 0.19%, respectively.

[36] The range of regional estimates of contrail cover shows variation in coverage of over 50% between different estimates and the lack of detailed coverage observations and their variability does not allow us to assess our parameter-

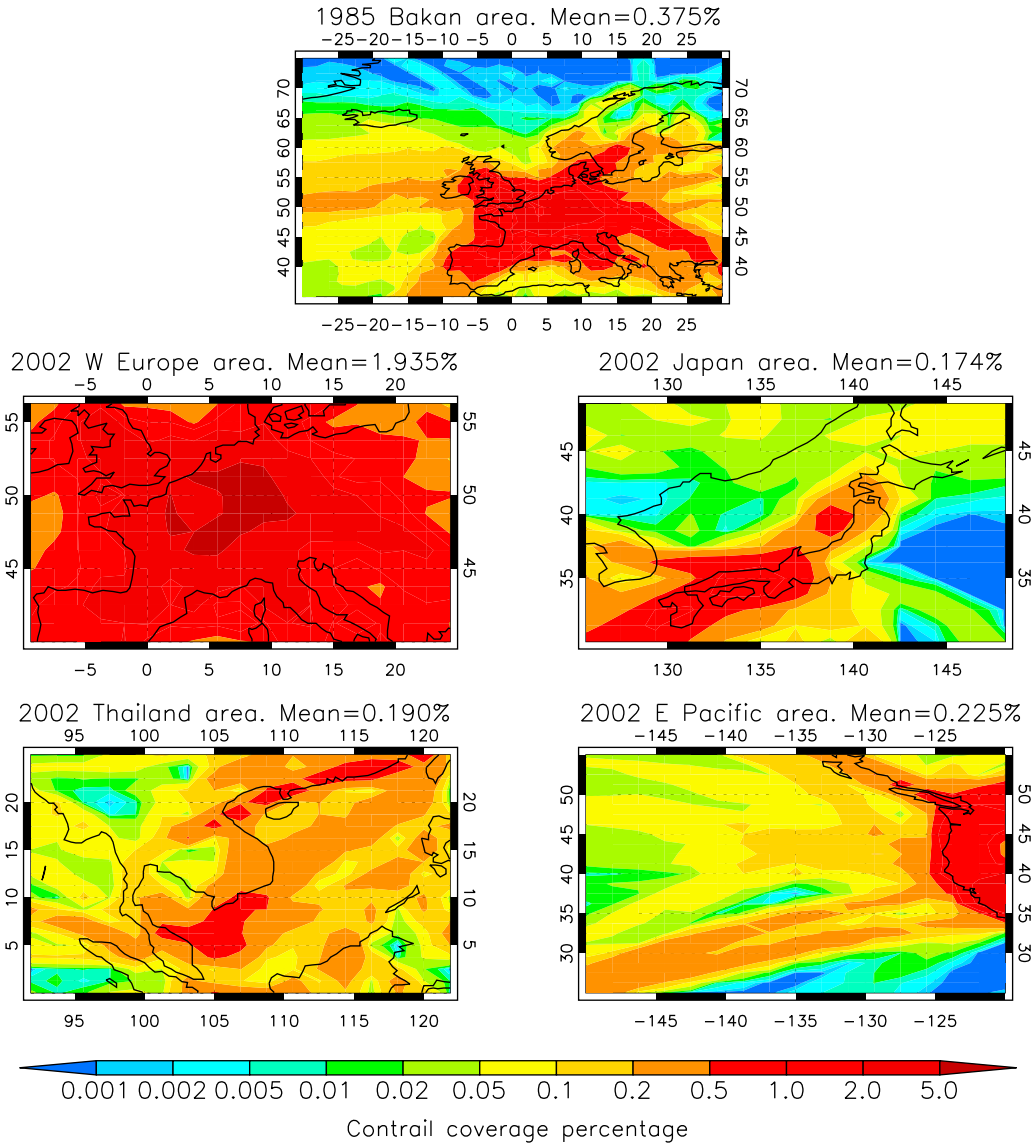

Figure 2. Regional contrail coverage estimates (%) produced by the model for (top) the "Bakan" area of 30°W to 30°E and 35°N to 75°N, (middle left) the western Europe area of 10°W to 23°E and 40°N to 56°N, (middle right) the Japan area of 125.625°E to 148.125°E and 29.689°N to 48.245°N, (bottom left) the Thailand area of 91.88°E to 121.875°E and 0°N to 25°N, and (bottom right) the eastern Pacific area of 120°W to 150°W and 25°N to 55°N.

ization at a regional scale in any robust manner. However, we can say that our parameterization finds similar broad regional variations in coverage with these previous estimates.

[37] In terms of global contrail coverage, the distribution produced by the current study is illustrated by Figure 3. As expected, the contrail cover pattern follows that of the most intense air traffic, with maxima in North America, Europe and East Asia. The parameterized value for the annual mean global coverage is 0.11% for 2002 air traffic, which is in relatively good agreement with other recent studies. Table 4 shows a comparison between this study and other studies for global and some regional values of contrail coverages. Taking into consideration the different underlying GCM and flight data used in order to estimate the contrail cover, it can be stated that the agreement between these results is fairly good.

[38] Figure 4 illustrates the twelve monthly means for two quantities: (1) the parameterized global contrail coverage averaged for the five simulated years and (2) the air traffic (distance flown) as reported by the AERO2K inventory. The coverages for each of the simulated years are also shown. As expected intuitively, it can be seen that there is a good correlation between the two quantities, with more traffic usually leading to higher contrail coverage. However, there are some exceptions such as the fact that although the air traffic recorded in June is very similar with the one from September, the June mean contrail coverage is larger than the September mean coverage by almost 20%. This is

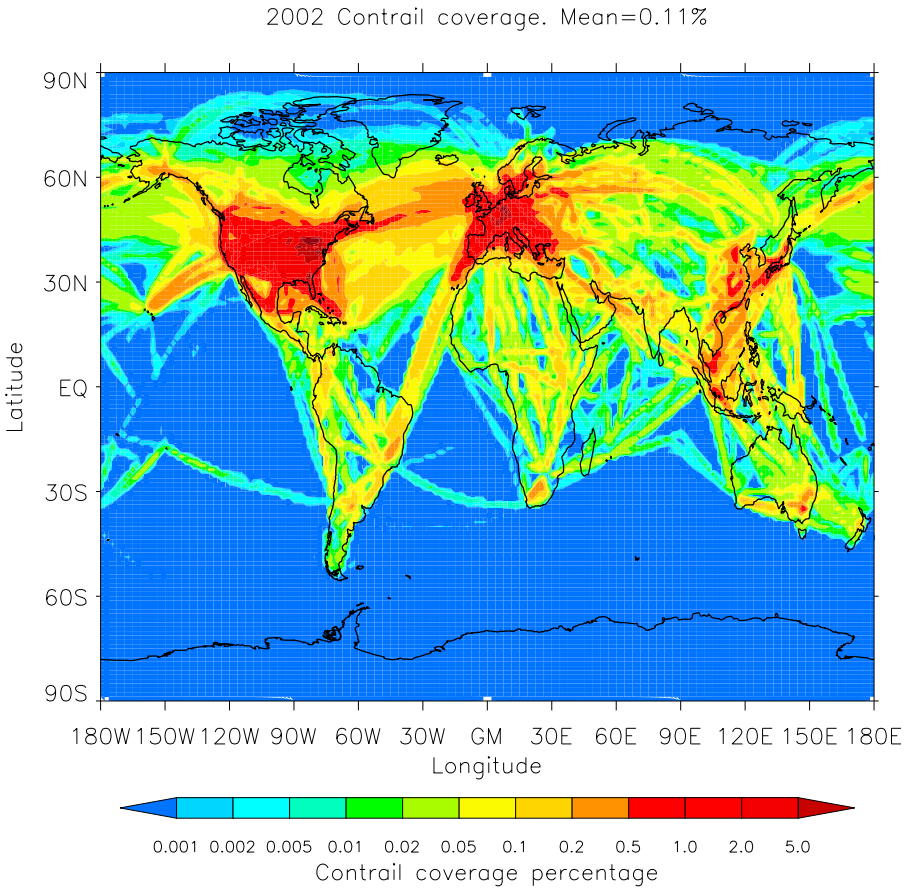

Figure 3. Annual mean global contrail coverage (%) for the 2002 air traffic.

caused by the fact that the contrail formation is affected by two independent factors, one being the amount of air traffic, and the other one being the ambient meteorological conditions. Thus, if the winter months correspond to low air traffic (with a minimum in December) and the summer months correspond to high air traffic (with a maximum in August), the meteorological conditions are less favorable to contrail formation in the three summer months, mainly because in these months the northern hemisphere midlatitudes upper troposphere relative humidity reaches its minimum [*Marquart et al.*, 2004; *Stuber and Forster*, 2007]. The combination of these two independent factors results in the largest global monthly mean contrail coverages being recorded in June and October.

4. Contrail Optical Depth

[39] As explained in section 1, the contrail radiative forcing does not only depend on coverage, but also on the contrail properties, particularly its optical depth. This induces a large uncertainty in any forcing estimate due to the fact that most models can only account for very limited variation in optical properties and that such variations are poorly constrained by observations.

[40] One of the greatest strengths of our parameterization is exactly its ability to allow for a variable optical depth,

Table 4. Averaged Contrail Coverage Estimate in the Published Literature Compared With Our Own Evaluation[a]

Region	Reference	Contrail Coverage for Traffic of Given Year (%)	
		1985	2002
"Bakan"	*Bakan et al.* [1994]	0.375	
West Europe	*Bakan et al.* [1994]	0.7	
	Meyer et al. [2002]	0.5	
	Stuber and Forster [2007]	0.9	
	this study	0.97	1.94
East Pacific	*Minnis et al.* [2005]		0.31
	Rädel and Shine [2008]		0.27
	this study	0.12	0.23
Japan	*Meyer et al.* [2007]	0.17	0.25
	this study	0.09	0.17
Thailand	*Meyer et al.* [2007]	0.06	0.13
	this study	0.09	0.19
All globe	*Minnis et al.* [1999]	0.09	
	Myhre and Stordal [2001]	0.09	
	Ponater et al. [2002]	0.07	
	Marquart et al. [2003]	0.06	
	Fichter et al. [2005]	0.047	
	Stuber and Forster [2007]	0.04	
	Rädel and Shine [2008]	0.04	0.08
	this study	0.055	0.11

[a]Values from *Meyer et al.* [2007] are climate model results corresponding to the year 1985, according to the notion of the present paper.

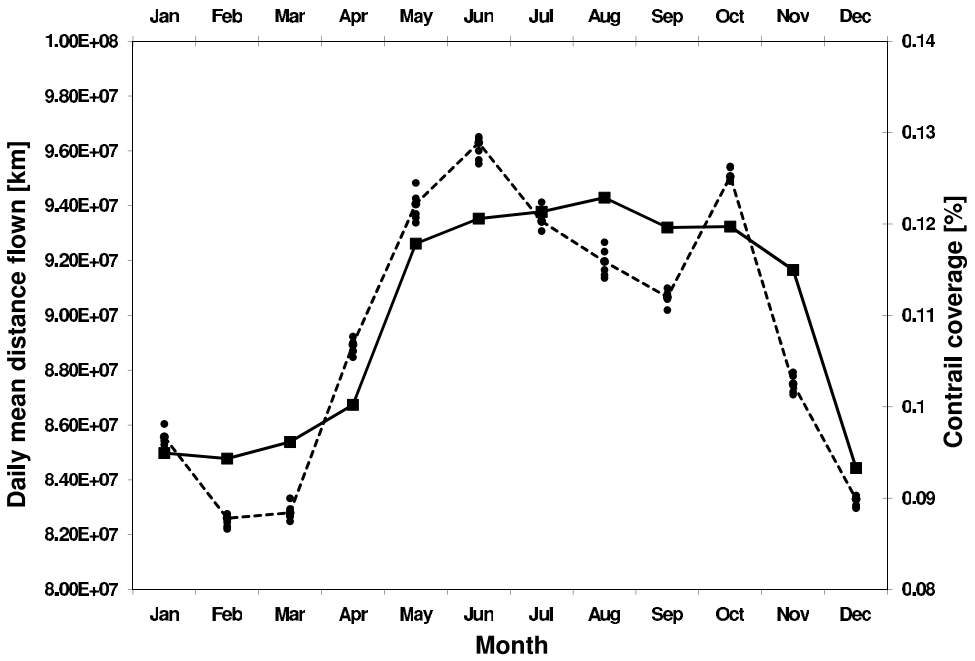

Figure 4. Monthly mean estimates of globally averaged daily distance flown (kilometers) (solid curve) and average linear contrail coverage of the five simulated years (%) (dashed curve) corresponding to the 2002 air traffic. The black dots indicate linear contrail coverage values for each of the five simulated years.

along with a variable contrail coverage. However, before being used in the radiative calculations, this variable optical depth needs to be scaled in order to match some observations, in a similar way to the scaling of the contrail fraction. This process is done by fixing the global mean optical depth to some specific values. For most estimations presented in this study, this fixed global mean optical depth is set to a value of 0.2, but sensitivity studies with other global mean values are also investigated in section 5.2.

[41] Mean contrail optical depths over the United States of America (USA) appear to be around 0.3 [see *Palikonda et al.*, 2005]. However, European contrail optical depths are observed to have a mean optical depth around 0.1 [*Meyer et al.*, 2002]. A recent modeling study suggests a global median optical depth of around 0.2 [*Kärcher et al.*, 2009]. Figure 5, constrained to a global mean optical depth of 0.2, shows higher optical depths over the USA than Europe and these are the right magnitudes as suggested by the *Palikonda et al.* [2005] and *Meyer et al.* [2002] observations. These patterns are also broadly consistent with *Ponater et al.* [2002]. Both studies find high optical depths in tropical regions, eastern United States and southeast Asia and low optical depth over Europe, northern Asia, Canada and the North Atlantic. Differences exist over northern Africa and most of Australia, where our optical depths are smaller. Mean optical depths larger than 0.5 are found in several regions within the western Pacific, Indian Ocean and the eastern Pacific region close to Central America.

5. Contrail Radiative Forcing

[42] In this section, we present the results obtained for the contrail RF when using the contrail coverage and optical depth distributions generated by our model and both the off-line and the on-line versions of the Edwards-Slingo code.

5.1. Off-Line Radiative Forcing Calculations

[43] The 5 year average parameterized contrail coverage distribution presented in section 3 and the contrail optical depth presented in section 4 is used together with the assumption of a constant contrail generalized effective size $D_{ge} = 30\mu$m within the off-line Edwards-Slingo code with the 144 (longitude) × 72 (latitude) × 23 (altitude) resolution. This off-line radiation code employs a monthly averaged climatology based on the ECMWF reanalysis data and cloud data from the International Satellite Cloud Climatology Project (ISCCP) archive.

[44] The model is run for each of the twelve calendar months, producing monthly averages for the contrail forcings. The geographical distribution of the forcings follows very closely the coverage distribution, with the highest values located in North America, Europe, and eastern Asia. The clear-sky annual global mean LW, SW, and net RFs are 28.4, −14.6 and 13.8 mW m^{-2}, respectively, while the all-sky values are 21.0, −9.0 and 12.0 mW m^{-2}, respectively. These values are broadly consistent with the ones reported by other studies (see Table 5) if we take into consideration the fact that we used a global mean optical depth of 0.2, compared with the values of 0.1 employed by *Marquart et al.* [2003], *Fichter et al.* [2005] and *Stuber and Forster* [2007], or 0.15 employed by *Rädel and Shine* [2008]. We should also mention that our estimates for the LW, SW and net RFs halved when the global mean optical depth was reduced from 0.2 to 0.1.

[45] Figure 6 illustrates zonal mean annual averages of the top of the atmosphere RFs for both clear-sky and all-sky

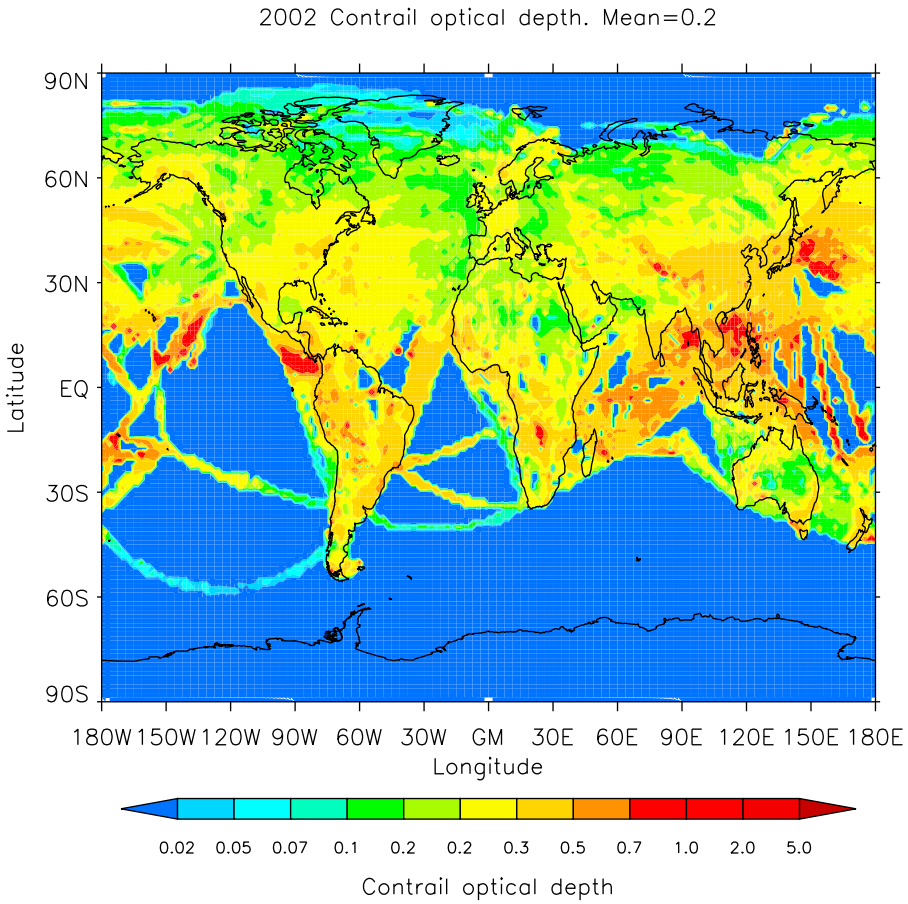

Figure 5. Annual mean global contrail optical depth integrated vertically across the atmosphere for the 2002 air traffic.

conditions. The strong cancellation of the LW and SW cloud masking effects means that the daily average contrail net RF is reduced by natural clouds by only approximately 13%, although the LW and SW forcings are reduced by more than 25% and 38%, respectively. This is consistent with the 10% net RF reduction reported by *Rädel and Shine* [2008].

[46] Another interesting point is that although the daily average net RF seems to be always positive, the daytime average net forcing takes some negative values for latitudes between 45N and 60N. This is better illustrated by Figure 7, which shows the daytime, nighttime and daily average net RFs for both clear-sky and all-sky cases. The possibility of negative net forcings in the daytime mean is consistent with findings from *Stuber et al.* [2006] and *Myhre et al.* [2010].

Table 5. Annual Global Mean All-Sky Radiative Forcings Estimated by Various Studies

Reference	Radiative Forcing for Traffic of Given Year (mW m^{-2})	
	1985	2002
Minnis et al. [1999]	8.0	-
Myhre and Stordal [2001]	9.0	15.0
Marquart et al. [2003]	3.5	6.0
Fichter et al. [2005]	3.2	-
Stuber and Forster [2007]	2.0	2.8
Rädel and Shine [2008]	-	5.9
This study, off-line	6.0	12.0
This study, on-line	3.9	7.7

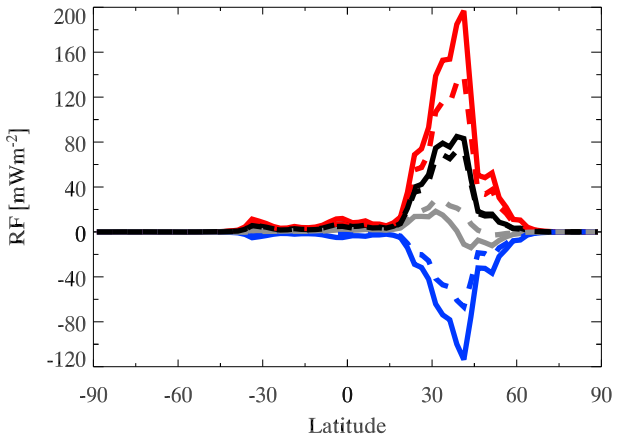

Figure 6. Zonal means of contrail LW (red lines), SW (blue lines), daytime average net (gray lines), and daily average net (black lines) RFs (W m^{-2}) for the 2002 air traffic obtained using the off-line model in clear-sky (solid lines) and all-sky (dashed lines) conditions.

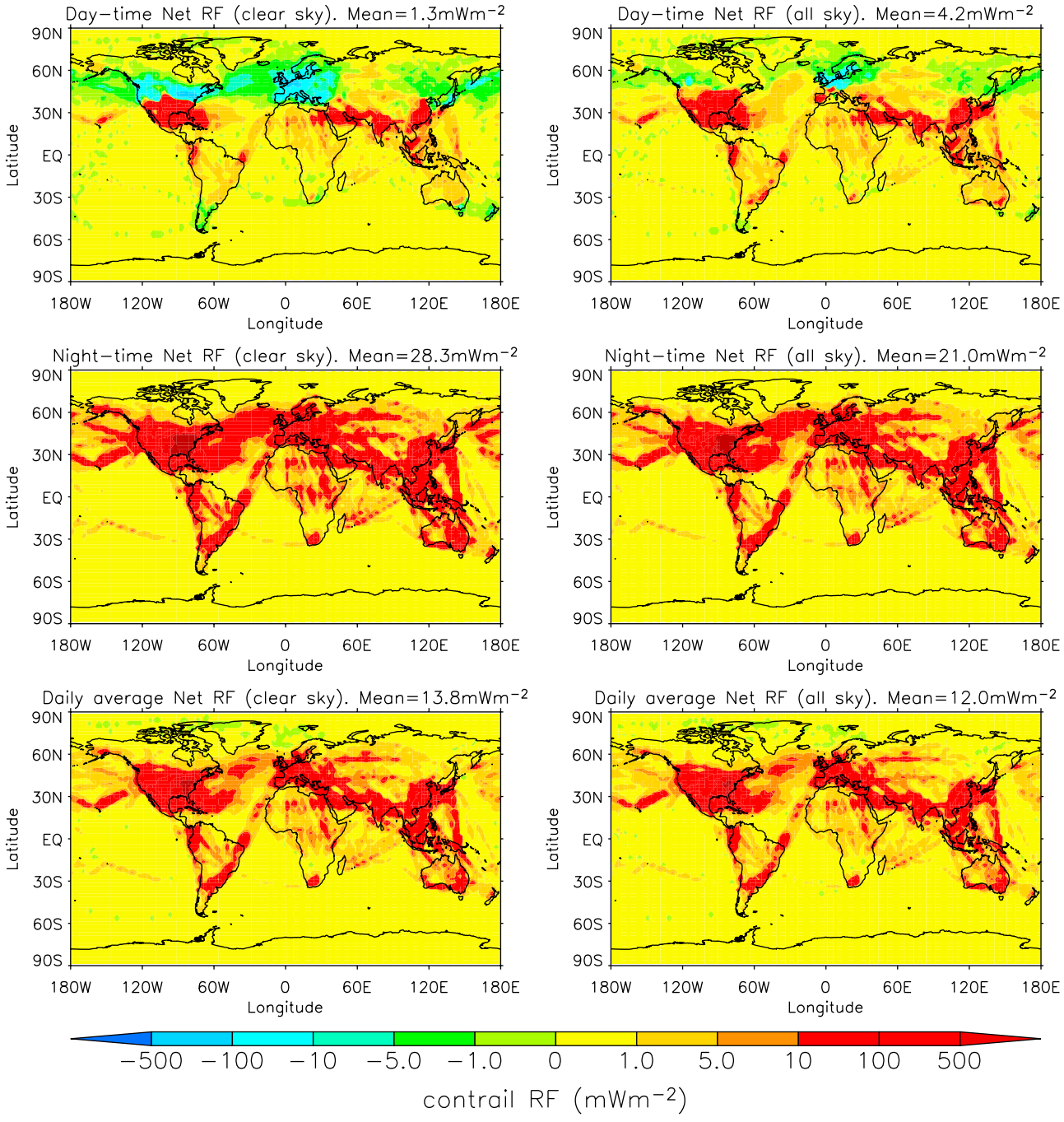

Figure 7. Net RF (mW m^{-2}) at the top of the atmosphere from the off-line model for the 2002 air traffic. (top) Daytime average, (middle) nighttime average, and (bottom) daily average for (left) clear-sky forcings and (right) all-sky forcings.

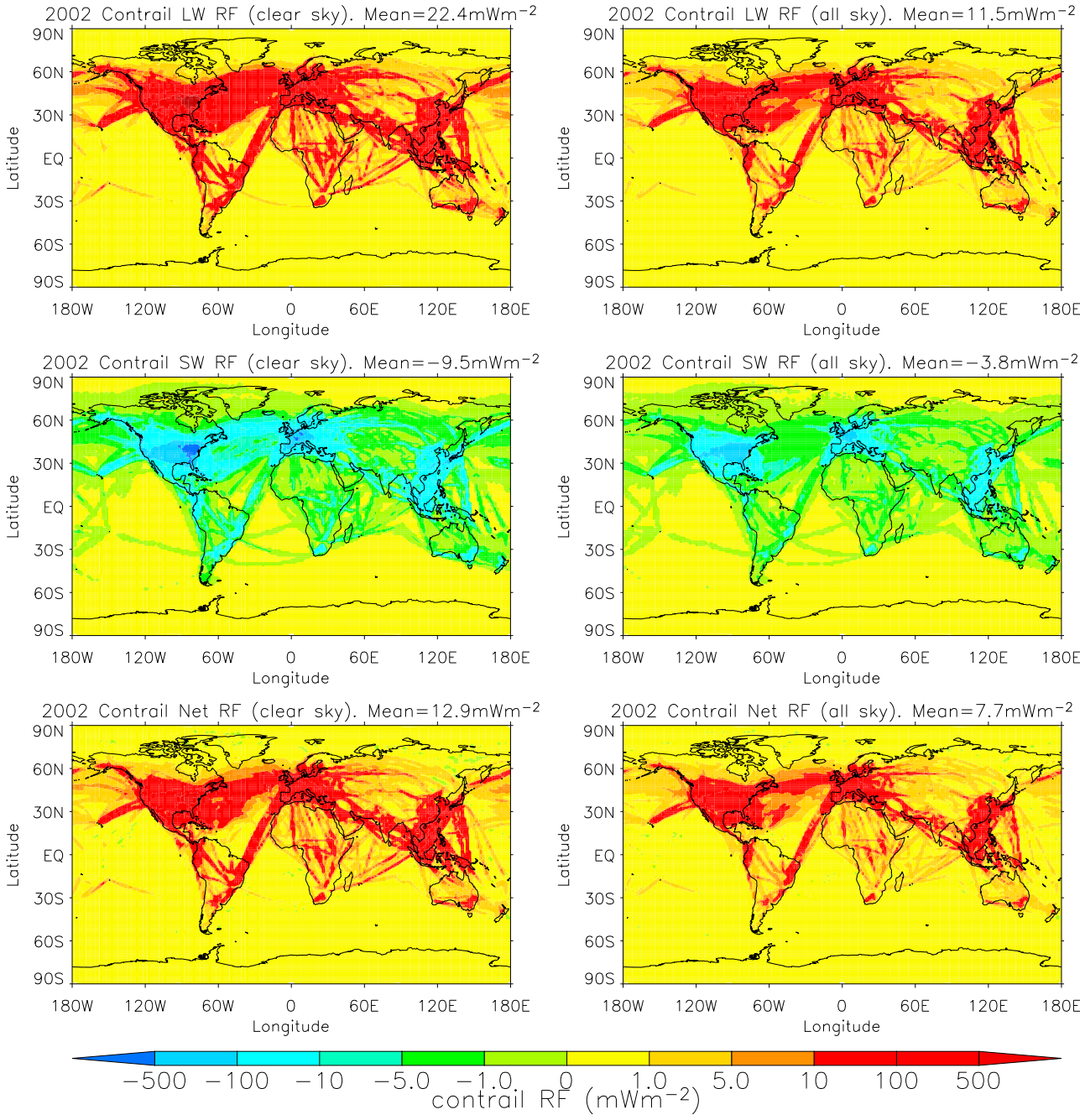

Figure 8. Radiative forcing (mW m^{-2}) at the top of the atmosphere from the on-line model for the 2002 air traffic. (top) Longwave, (middle) shortwave, and (bottom) net for (left) clear-sky forcings and (right) all-sky forcings.

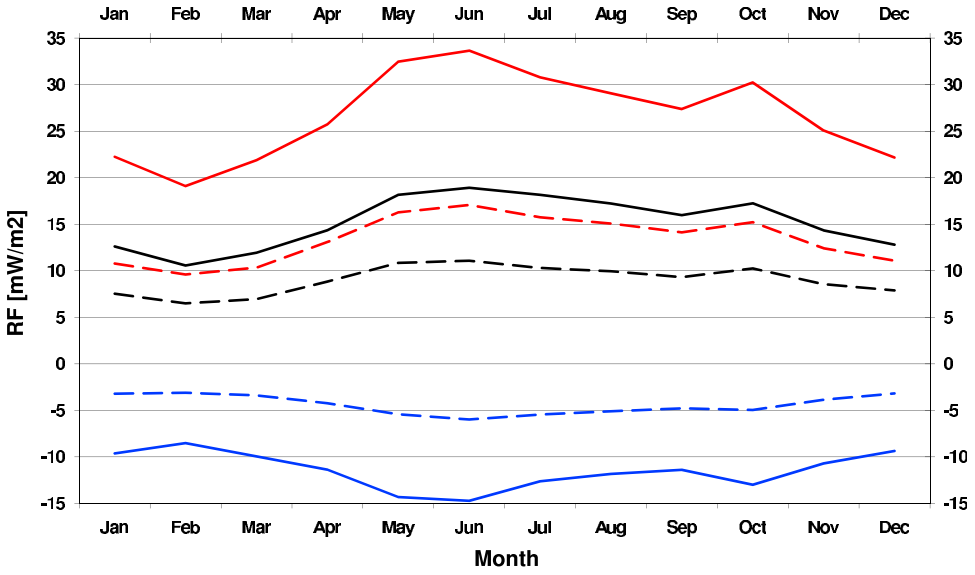

Figure 9. Globally averaged radiative forcing by month from the on-line model. Longwave (red lines), shortwave (blue lines), and net (black lines). Clear-sky (solid lines) and all-sky (dashed lines).

5.2. On-Line Radiative Forcing Calculations

[47] One of the main advantages of the current parameterization scheme is the fact that it allows the estimation of the contrail RFs using the HadGEM2 on-line version of the Edwards-Slingo radiation code, with a 192 (longitude) × 145 (latitude) × 38 (altitude) resolution. Figure 8 illustrates the RFs estimated in this way. The clear-sky annual global mean LW, SW, and net RFs are 22.4, −9.5 and 12.9 mW m^{-2}, respectively, while the all-sky values are 11.5, −3.8 and 7.7 mW m^{-2}, respectively (see Table 6). In clear-sky conditions both the geographical distribution and the magnitude of the RFs are similar to those obtained when using the off-line version of the model. However, in the all-sky case, although the same geographical pattern is maintained, the forcings are reduced by significant amounts. The LW and SW forcings in all-sky conditions are reduced by approximately 50% and 60%, respectively, compared to the clear-sky forcings. This results in the all-sky net RF being reduced by approximately 40%, compared to the clear-sky net RF. This significant influence of natural clouds on the contrail RF has not been observed when the off-line model was employed, nor has it been reported by other studies [e.g., *Marquart et al.*, 2003; *Stuber and Forster*, 2007; *Rädel and Shine*, 2008] that showed a much smaller impact of natural clouds. Figure 9 plots the twelve monthly global mean contrail RFs and shows that this effect is clearly a significant feature throughout the whole calendar year. We do not believe that these differences are caused by our treatment of contrail as aerosol as this treatment should minimize contrail-natural cloud overlap, thereby decreasing clear-sky and all-sky differences. Also, our results suggest that this enhancement is not occurring in the *Marquart et al.* [2003] study, particularly as they employ a maximum random overlap scheme [*Marquart and Mayer*, 2002] that should make these clear-sky-cloudy sky differences more pronounced. Yet they only find a 10% difference between clear and cloudy sky net forcing, which they interpret to be somewhat like a maximum effect that the presence of natural clouds may have on the contrail forcing.

[48] The significant decrease in forcing when natural cloud is introduced into the on-line model does not occur in the off-line model version. Although these two models employ different meteorologies and resolutions that give different absolute forcing values, we focus on relative differences between their clear-sky and all-sky forcings to understand this cloud effect. In the off-line case the RF calculations are performed only once every month (although they include the diurnal cycle of the solar zenith angle), using monthly means for all the parameters involved in the calculations, while in the on-line case the RF calculations are performed at every radiation scheme time step, i.e., every 3 h. This means that variability in parameters such as the contrail cover, or the natural cloud amount, on time scales shorter than one month, and correlations between them are accounted for only by the on-line version of the code. Such variabilities can be quite significant, from a radiative forcing point of view, and their inclusion into a contrail parameterization is expected to produce better estimates, compared to parameterizations that excludes them.

[49] Figure 10 shows a map of linear Pearson correlation coefficients between time series of two model parameters from a September run with a time resolution of 3 h: (1) two-dimensional natural cloud fraction between 8.82 and 12.5 km

Table 6. Annual Global Mean Contrail Radiative Forcing From the Off-Line and On-Line Calculations for the 2002 Air Traffic[a]

	Clear Sky			All Sky		
	LW	SW	Net	LW	SW	Net
Off-line model	28.4	−14.6	13.8	21.0	−9.0	12.0
On-line model	22.4	−9.5	12.9	11.5	−3.8	7.7

[a]Unit is mW m^{-2}.

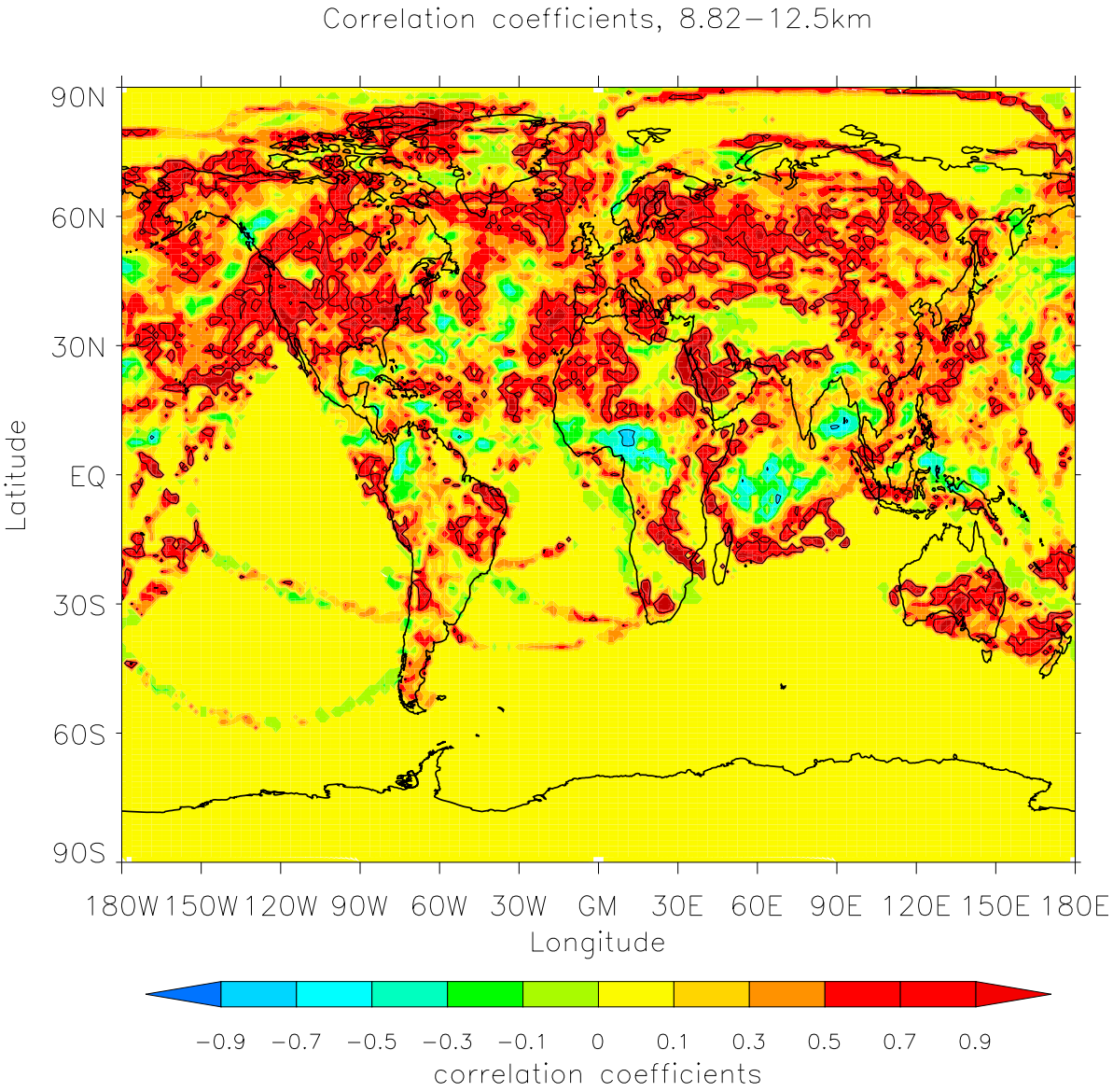

Figure 10. Linear Pearson correlation coefficients for time series of model cloud fraction and model contrail fraction in the on-line model. Black isolines show areas with values below −0.7 or above 0.7.

altitude and (2) two-dimensional contrail fraction. It is observed that there are several regions with correlation coefficients larger than 0.7, meaning that in the model there is a correlation between the contrail formation and natural clouds. We believe that this correlation is the main explanation for the strong reduction in all-sky contrail RFs that is observed when using the on-line parameterization, but is missed out by the off-line parameterizations.

[50] As already explained in section 5.1, although our parameterization does not assume a constant contrail optical depth, it still needs an a priori choice for the value of the global mean contrail optical depth. This choice is bound to have a significant effect on the contrail RF estimates. Table 7 shows the RFs obtained for three different global mean optical depths, in both clear-sky and all-sky conditions. It is observed that the dependence of contrail RF on global mean contrail optical depth is almost linear, which is consistent with sensitivity studies presented by *Marquart et al.* [2003], *Stuber and Forster* [2007], and *Rädel and Shine* [2008]. This also confirms the fact that improving observations for contrail optical depth is a priority to accurately estimate contrail RF. The global mean contrail optical depth is not

Table 7. Annual Global Mean Contrail Radiative Forcing for Different Mean Optical Depths in the On-Line Model for the 2002 Air Traffic[a]

Global Mean Optical Depth	Clear Sky			All Sky		
	LW	SW	Net	LW	SW	Net
0.1	13.2	−6.9	6.3	6.3	−2.4	3.9
0.2	22.4	−9.5	12.9	11.5	−3.8	7.7
0.3	32.1	−12.7	19.4	17.1	−5.5	11.6

[a]Unit is mW m^{-2}.

well constrained by observations, although it is likely to be smaller than 0.3 (see section 4).

6. Discussion and Conclusions

[51] The accuracy of a contrail RF estimation is highly dependent on how realistic the contrail coverage and optical properties estimates are, as well as natural cloudiness. The large majority of the current contrail RF estimates have been made using simple parameterizations within radiative transfer models that employ monthly averaged cloud data and/or assume constant optical depths. Averaging cloud data over a month does not fully account for correlations between natural cloud and contrail on shorter time scales, and therefore reduces the ability to produce accurate contrail RF estimates. A next step in improving these estimates is the use of GCMs as they have the important advantage of accounting for the short time scale variability of contrail properties dependent on the actual ambient conditions.

[52] The HadGEM2 GCM with the contrail parameterization described in this paper is the only other GCM with a built-in on-line contrail parameterization, apart from the ECHAM4 model, for which two contrail parameterizations have been developed, namely that of *Ponater et al.* [2002] and the recent *Burkhardt and Kärcher* [2009] contrail cirrus parameterization. Although our parameterization follows a methodology inspired by *Ponater et al.* [2002], there are some significant differences between the two schemes, since they are hosted in two very different climate models. One main difference is the formulae for calculating the potential contrail coverages. In each scheme this formula is a modified form of the parameterization of the natural cirrus coverage in the respective host models. Another main difference is the radiative transfer parameterization from these two GCMs. While ECHAM4 follows the *Fouquart and Bonnel* [1980] and *Morcrette* [1989] parameterizations for the SW and LW part of the spectrum, respectively, HadGEM2 follows the *Edwards and Slingo* [1996] parameterization. Apart from these two main methodological differences, it should also be noted that the two schemes also employ different air traffic inventories. All this means that we now have estimates for contrail coverage and RF from two independent GCMs, which will certainly help to consolidate our knowledge of contrail impact on climate.

[53] As noted in section 3, the annual mean global linear contrail coverage estimate, i.e., 0.11% for the 2002 air traffic, made by our parameterization is in good agreement with the published work from other studies. We estimate that for global mean optical depth of 0.1 and 0.2, the all-sky globally averaged persistent linear contrail forcing is 3.9 mW m^{-2} and 7.7 mW m^{-2}, respectively; the corresponding clear-sky values are 6.3 mW m^{-2} and 12.9 mW m^{-2}, respectively. Our parameterization makes a range of assumptions regarding contrail coverage, optical depth, optical properties and contrail-cloud overlap. Where possible, using sensitivity tests, we have examined how optical depth, optical properties and contrail coverage observations impact our results. Provided the current observations of contrail optical depth and the regional satellite derived contrail coverages employed in our parameterization are correct, our calculated globally averaged persistent linear contrail forcing of less than 10 mW m^{-2} appears likely.

[54] An important finding of this study is the fact that, when incorporating day to day variations in cloud cover, we observe that contrails seem to preferentially form when background natural cloud cover is higher. While this might be expected because regions of high relative humidity are likely to be preferential formation areas for both naturally occurring cirrus and persistent contrails, this acts to limit the radiative impact of any contrails formed, due to the natural cloud masking effect. Thus, the inclusion of day-to-day variability into contrail forcing calculations may reduce global mean forcing estimates by about 40%. This is a significant new result, as previous studies have not evaluated this effect.

[55] Future improvement of the current work should follow two different routes. The first one should focus on improving current contrail coverage and optical properties observations, as in the current methodology they both play essential roles. The second route should be the development of new parameterizations for spreading contrail cirrus clouds, which would prevent the need for using sometimes subjective contrail coverage estimates to scale forcing and climate impact estimates. Until these improvements are achieved, the current parameterization is expected to be the most suitable tool for assessing the impact of linear contrails on climate.

[56] **Acknowledgments.** The authors would like to thank Steven Dobbie and the three anonymous referees for their careful review of the manuscript and useful comments and suggestions. The work of A.R. and P.M.F. was supported by the Omega partnership under the project code Ω 1/009. The work of A.J., O.B., J.M.H., and N.B. was supported by the Joint DECC, Defra, and MoD Integrated Climate Programme: DECC/Defra (GA01101), MoD (CBC/2B/0417 Annex C5).

References

Appleman, H. (1953), The formation of exhaust condensation trails by jet aircraft, *Bull. Am. Meteorol. Soc.*, *34*, 14–20.

Bakan, S., M. Betancor, V. Gayler, and H. Grassl (1994), Contrail frequency over Europe from NOAA-satellite images, *Ann. Geophys.*, *12*(10–11), 962–968.

Burkhardt, U., and B. Kärcher (2009), Process-based simulation of contrail cirrus in a global climate model, *J. Geophys. Res.*, *114*, D16201, doi:10.1029/2008JD011491.

Burkhardt, U., B. Kärcher, M. Ponater, K. Gierens, and A. Gettelman (2008), Contrail cirrus supporting areas in model and observations, *Geophys. Res. Lett.*, *35*, L16808, doi:10.1029/2008GL034056.

Collins, W., et al. (2008), Evaluation of the HadGEM2 model, *Hadley Cent. Tech. Note 74*, Met Off., Exeter, U. K.

Edwards, J., and A. Slingo (1996), Studies with a flexible new radiation code. 1. Choosing a configuration for a large-scale model, *Q. J. R. Meteorol. Soc.*, *122*, 689–719.

Eyers, C., P. Norman, J. Middel, M. Plohr, S. Michot, K. Atkinson, and R. Christou (2004), AERO2k global aviation emissions inventories for 2002 and 2025, *Tech. Rep. Qinetiq/04/01113*, QinetiQ Ltd., Farnborough, U. K.

Fichter, C., S. Marquart, R. Sausen, and D. Lee (2005), The impact of cruise altitude on contrails and related radiative forcing, *Meteorol. Z.*, *14*, 563–572.

Forster, P., et al. (2007), Changes in atmospheric constituents and in radiative forcing, in *Climate Change 2007: The Physical Science Basis. Contribution of Working Group I to the Fourth Assessment Report of the Intergovernmental Panel on Climate Change*, edited by S. Solomon et al., pp. 131–234, Cambridge Univ. Press, Cambridge, U. K.

Fouquart, Y., and B. Bonnel (1980), Computations of solar heating of the Earth's atmosphere: A new parameterization, *Beitr. Phys. Atmos.*, *53*, 35–62.

Fu, Q. (1996), An accurate parameterization of the solar radiative properties of cirrus clouds for climate models, *J. Clim.*, *9*, 2058–2082.

Fu, Q., B. Carlin, and G. Mace (2000), Cirrus horizontal inhomogeneity and OLR bias, *Geophys. Res. Lett.*, *27*, 3341–3344.

Hurrell, J., J. Hack, D. Shea, J. Caron, and J. Rosinski (2008), A new sea surface temperature and sea ice boundary dataset for the Community Atmosphere Model, *J. Clim.*, *21*, 5145–5153.

Kärcher, B., U. Burkhardt, S. Unterstrasser, and P. Minnis (2009), Factors controlling contrail cirrus optical depth, *Atmos. Chem. Phys. Discuss.*, *9*, 11,589–11,658.

Lohmann, U., and B. Kärcher (2002), First interactive simulations of cirrus clouds formed by homogeneous freezing in the ECHAM general circulation model, *J. Geophys. Res.*, *107*(D10), 4105, doi:10.1029/2001JD000767.

Mannstein, H., R. Meyer, and P. Wendling (1999), Operational detection of contrails from NOAA–AVHRR-data, *Int. J. Remote Sens.*, *20*(8), 1641–1660.

Marquart, S., and B. Mayer (2002), Towards a reliable GCM estimation of contrail radiative forcing, *Geophys. Res. Lett.*, *29*(8), 1179, doi:10.1029/2001GL014075.

Marquart, S., M. Ponater, F. Mager, and R. Sausen (2003), Future development of contrail cover, optical depth, and radiative forcing: Impacts of increasing air traffic and climate change, *J. Clim.*, *16*, 2890–2904.

Marquart, S., M. Ponater, F. Mager, and R. Sausen (2004), Future development of contrails: Impacts of increasing air traffic and climate change, paper presented at Conference on Aviation, Atmosphere and Climate, Eur. Communities, Friedrichshafen, Germany.

Martin, G., M. Ringer, V. Pope, A. Jones, C. Dearden, and T. Hinton (2006), The physical properties of the atmosphere in the new Hadley Centre Global Environmental Model (HadGEM1). Part I: Model description and global climatology, *J. Clim.*, *19*, 1274–1301.

Meerkötter, R., U. Schumann, D. Doelling, P. Minnis, T. Nakajima, and Y. Tsushima (1999), Radiative forcing by contrails, *Ann. Geophys.*, *17*(8), 1080–1094.

Meyer, R., H. Mannstein, R. Meerkötter, U. Schumann, and P. Wendling (2002), Regional radiative forcing by line-shaped contrails derived from satellite data, *J. Geophys. Res.*, *107*(D10), 4104, doi:10.1029/2001JD000426.

Meyer, R., R. Buell, C. Leiter, H. Mannstein, S. Pechtl, T. Oki, and P. Wendling (2007), Contrail observations over southern and eastern Asia in NOAA/AVHRR data and comparisons to contrail simulations in a GCM, *Int. J. Remote Sens.*, *28*(9), 2049–2069.

Minnis, P., U. Schumann, D. Doelling, K. Gierens, and D. Fahey (1999), Global distribution of contrail radiative forcing, *Geophys. Res. Lett.*, *26*, 1853–1856.

Minnis, P., R. Palikonda, B. Walter, J. Ayers, and H. Mannstein (2005), Contrail properties over the eastern North Pacific from AVHRR data, *Meteorol. Z.*, *14*, 515–523.

Morcrette, J.-J. (1989), Description of the radiation scheme in the ECMWF model, *Tech. Memo. 165*, 26 pp., ECMWF, Reading, U. K.

Myhre, G., and F. Stordal (2001), On the tradeoff of the solar and thermal infrared radiative impact of contrails, *Geophys. Res. Lett.*, *28*, 3119–3122.

Myhre, G., et al. (2010), Intercomparison of radiative forcing calculations of stratospheric water vapour and contrails, *Meteorol. Z.*, *18*, 585–596, doi:10.1127/0941-2948/2009/0411.

Palikonda, R., P. Minnis, D. Duda, and H. Mannstein (2005), Contrail coverage derived from 2001 AVHRR data over the continental United States of America and surrounding areas, *Meteorol. Z.*, *14*, 525–536.

Ponater, M., S. Marquart, and R. Sausen (2002), Contrails in a comprehensive global climate model: Parameterization and radiative forcing results, *J. Geophys. Res.*, *107*(D13), 4164, doi:10.1029/2001JD000429.

Rädel, G., and K. Shine (2008), Radiative forcing by persistent contrails and its dependence on cruise altitudes, *J. Geophys. Res.*, *113*, D07105, doi:10.1029/2007JD009117.

Schmidt, E. (1941), Die Entstehung von Eisnebel aus den Auspuffgasen von Flugmotoren, in *Deutschen Akademie der Luftfahrtforschung*, vol. 44, pp. 1–15, Verlag R. Oldenbourg, Munich, Germany.

Schumann, U. (1996), On conditions for contrail formation from aircraft exhausts, *Meteorol. Z.*, *5*, 4–23.

Smith, R. (1990), A scheme for predicting layer clouds and their water content in a general circulation model, *Q. J. R. Meteorol. Soc.*, *116*, 435–460.

Strauss, B., R. Meerkötter, B. Wissinger, P. Wendling, and M. Hess (1997), On the regional climatic impact of contrails: Microphysical and radiative properties of contrails and natural cirrus clouds, *Ann. Geophys.*, *15*(11), 1457–1467.

Stuber, N., and P. Forster (2007), The impact of diurnal variations of air traffic on contrail radiative forcing, *Atmos. Chem. Phys.*, *7*(12), 3153–3162.

Stuber, N., P. Forster, G. Rädel, and K. Shine (2006), The importance of the diurnal and annual cycle of air traffic for contrail radiative forcing, *Nature*, *441*(7095), 864–867.

Waliser, D., et al. (2009), Cloud ice: A climate model challenge with signs and expectations of progress, *J. Geophys. Res.*, *114*, D00A21, doi:10.1029/2008JD010015.

Wilson, D. (2007), The large-scale cloud scheme and saturated specific humidity, *Unified Model Doc. Pap. 29*, Met Office, Exeter, U. K.

Wilson, D., and D. Gregory (2003), The behaviour of large-scale model cloud schemes under idealized forcing scenarios, *Q. J. R. Meteorol. Soc.*, *129*, 967–986.

N. Bellouin, O. Boucher, J. M. Haywood, and A. Jones, Met Office Hadley Centre, FitzRoy Road, Exeter EX1 3PB, UK.

R. R. De Leon, Centre for Air Transport and the Environment, Manchester Metropolitan University, Manchester M1 5GD, UK.

P. M. Forster and A. Rap, Institute for Climate and Atmospheric Science, School of Earth and Environment, University of Leeds, Leeds LS2 9JT, UK. (a.rap@leeds.ac.uk)